

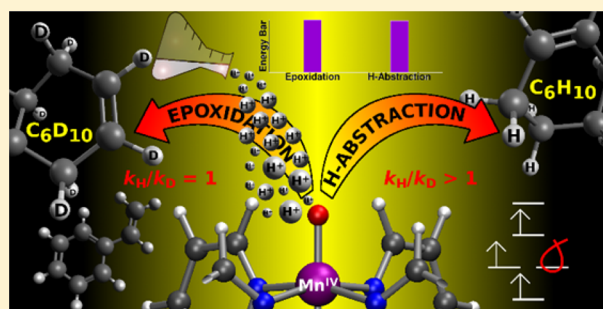
Factors Controlling the Chemoselectivity in the Oxidation of Olefins by Nonheme Manganese(IV)-Oxo Complexes

Surin Kim,[§] Kyung-Bin Cho,[§] Yong-Min Lee, Junying Chen, Shunichi Fukuzumi,* and Wonwoo Nam*

Department of Chemistry and Nano Science, Ewha Womans University, Seoul 03760, Korea

S Supporting Information

ABSTRACT: We report the oxidation of cyclic olefins, such as cyclohexene, cyclohexene-*d*₁₀, and cyclooctene, by mononuclear nonheme manganese(IV)-oxo (Mn^{IV}O) and triflic acid (HOTf)-bound Mn^{IV}O complexes. In the oxidation of cyclohexene, the Mn^{IV}O complexes prefer the C—H bond activation to the C=C double bond epoxidation, whereas the C=C double bond epoxidation becomes a preferred reaction pathway in the cyclohexene oxidation by HOTf-bound Mn^{IV}O complexes. In contrast, the oxidation of cyclohexene-*d*₁₀ and cyclooctene by the Mn^{IV}O complexes occurs predominantly via the C=C double bond epoxidation. This conclusion is drawn from the product analysis and kinetic studies of the olefin oxidation reactions, such as the epoxide versus allylic oxidation products, the formation of Mn(II) versus Mn(III) products, and the kinetic analyses. Overall, the experimental results suggest that the energy barrier of the C=C double bond epoxidation is very close to that of the allylic C—H bond activation in the oxidation of cyclic olefins by high-valent metal-oxo complexes. Thus, the preference of the reaction pathways is subject to changes upon small manipulation of the reaction environments, such as the supporting ligands and metal ions in metal-oxo species, the presence of HOTf (i.e., HOTf-bound Mn^{IV}O species), and the allylic C—H(D) bond dissociation energies of olefins. This is confirmed by DFT calculations in the oxidation of cyclohexene and cyclooctene, which show multiple pathways with similar rate-limiting energy barriers and depending on the allylic C—H bond dissociation energies. In addition, the possibility of excited state reactivity in the current system is confirmed for epoxidation reactions.



INTRODUCTION

High-valent metal-oxo (MO) species are highly reactive intermediates involved in the oxidation of organic substrates by heme and nonheme enzymes and their model compounds.^{1,2} In biomimetic studies, a number of mononuclear nonheme FeO and MnO complexes have been synthesized and characterized recently, and their reactivities have been investigated in various oxidation reactions, including C—H bond activation, oxygen atom transfer (OAT), and electron-transfer (ET) reactions.¹ In those studies, it has been shown that the reactivities and mechanisms of the MO species in oxidation reactions are influenced significantly by several factors, such as the supporting and axial ligands of the MO complexes, the spin states of the metal ions, and the binding of redox-inactive metal ions and protons to the MO moiety.² Especially, we have demonstrated that the binding of redox-inactive metal ions and protons by the mononuclear nonheme FeO and MnO complexes shifts their oxidation potentials positively, resulting in the significant increase of their oxidizing power and reactivities in OAT and ET reactions.^{2a,3,4}

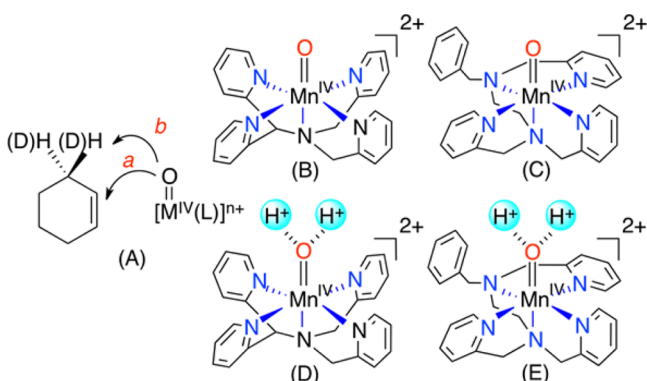
The chemoselectivity of C—H hydroxylation versus C=C epoxidation has been discussed in the oxidation of olefins by cytochromes P450, synthetic metalloporphyrins, and their high-valent MO models under catalytic and stoichiometric reaction conditions; the change of the chemoselectivity has been

proposed with the involvement of different reactive species (e.g., high-valent Fe^{IV}O porphyrin π -cation radical versus (Porp)Fe^{III}—OOH), temperature effects, electron-donating ability of axial ligands and/or electron-richness of porphyrin ligands.^{5–8} In some studies, cyclohexene has been used as a substrate probe for the determination of MO properties toward a hydrogen atom (H atom) abstraction from allylic C—H bonds or an OAT to the C=C double bond (Scheme 1A).^{6,7,9} By analyzing products formed in the cyclohexene oxidation reactions (e.g., cyclohexene oxide from C=C epoxidation versus cyclohexenol and cyclohexenone from C—H bond activation), reaction mechanism(s) toward the C—H bond activation versus C=C double bond epoxidation by MO complexes (or any other metal–oxygen species) has been proposed.^{5–8} Very recently, we have shown that mononuclear nonheme M^{IV}O (M = Fe and Ru) complexes prefer the C—H bond activation to the C=C double bond epoxidation in the oxidation of cyclohexene, giving allylic oxidation products exclusively (Scheme 1A, reaction pathway b).¹⁰ Interestingly, when cyclohexene was replaced by deuterated cyclohexene (cyclohexene-*d*₁₀), the C=C double bond epoxidation became viable, albeit not dominant, with an overall slow reaction rate

Received: June 17, 2016

Published: July 27, 2016

Scheme 1. Reactions Showing (a) C=C Double Bond Epoxidation and (b) C—H(D) Bond Activation by $Mn^{IV}O$ Species (A). Schematic Drawings of $[Mn^{IV}(O)(N4Py)]^{2+}$ (B), $[Mn^{IV}(O)(Bn-TPEN)]^{2+}$ (C), $[Mn^{IV}(O)(N4Py)]^{2+}$ —(HOTf)₂ (D), and $[Mn^{IV}(O)(Bn-TPEN)]^{2+}$ —(HOTf)₂ (E)



(Scheme 1A, reaction pathway *a*) and a minor epoxidation product yield. These results led us to propose that the change of reaction mechanisms (i.e., the preference of C—H bond activation versus the C=C double bond epoxidation) depends on the allylic C—H(D) bond dissociation energies (BDE) of the olefin substrates and that the C—H bond activation of cyclohexene by the MO complexes may include tunneling.^{10,11}

Continuing on this line of research, we turned our attention to mononuclear nonheme $Mn^{IV}O$ complexes that were synthesized recently and investigated in various oxidation reactions.^{12,13} The effects of Brønsted and Lewis acids on the reactivities of the $Mn^{IV}O$ complexes have also been discussed in the C—H bond activation, OAT, and ET reactions by $[Mn^{IV}(O)(N4Py)]^{2+}$ (N4Py = *N,N*-bis(2-pyridylmethyl)-*N*-bis(2-pyridyl)methylamine), $[Mn^{IV}(O)(Bn-TPEN)]^{2+}$ (Bn-TPEN = *N*-benzyl-*N,N',N'*-tris(2-pyridylmethyl)-1,2-diaminoethane), and their HOTf-bound $Mn^{IV}O$ complexes (see structures of B—E in Scheme 1).⁴ However, the oxidation of olefins by nonheme $Mn^{IV}O$ complexes has never been investigated previously. Moreover, the effect of Brønsted acid on the chemoselectivity in the oxidation of cyclic olefins by metal-oxo (MO) complexes, including $Mn^{IV}O$ complexes, has never been explored in both heme and nonheme systems. We therefore attempted the olefin oxidation reactions with the spectroscopically well-characterized $Mn^{IV}O$ complexes, $[Mn^{IV}(O)(N4Py)]^{2+}$ and $[Mn^{IV}(O)(Bn-TPEN)]^{2+}$,¹² and their HOTf-bound $Mn^{IV}O$ complexes.⁴ Herein, we report for the first time that nonheme $Mn^{IV}O$ complexes prefer the C—H bond activation over the C=C double bond epoxidation in the oxidation of cyclohexene (Scheme 1, reaction pathway *b* by B and C). We also report that the chemoselectivity on the C—H bond activation versus the C=C double bond epoxidation changes when the oxidation of cyclohexene by the $Mn^{IV}O$ complexes is carried out in the presence of HOTf (i.e., by HOTf-bound $Mn^{IV}O$ complexes); the C=C double bond epoxidation becomes a dominant pathway (Scheme 1, reaction pathway *a* by D and E). Moreover, we show that the oxidation of cyclohexene-*d*₁₀ and cyclooctene by the $Mn^{IV}O$ complexes occurs mainly via the C=C double bond epoxidation under any reaction conditions (Scheme 1, reaction pathway *a*), demonstrating that the allylic C—H bond strength and tunneling are determining factors for the chemoselectivity in the oxidation of cyclic olefins. Extensive theoretical calculations

were also performed to gain further understanding into the reaction mechanisms of the current systems, such as the oxidation of cyclohexene and cyclooctene by nonheme $Mn^{IV}O$ complexes. The present results provide valuable mechanistic insights into the oxidation of cyclic olefins by mononuclear nonheme $Mn^{IV}O$ complexes.

RESULTS AND DISCUSSION

Chemoselectivity in the Oxidation of Cyclohexene by Nonheme $Mn^{IV}(O)$ Complexes. The oxidation of olefins by $[Mn^{IV}(O)(N4Py)]^{2+}$ (**1**) and $[Mn^{IV}(O)(Bn-TPEN)]^{2+}$ (**2**) was investigated using cyclohexene as a substrate probe, to gauge the chemoselectivity on the C—H bond activation versus the C=C double bond epoxidation in $CF_3CH_2OH-CH_3CN$ ($\nu/\nu = 1:1$) at 25 °C. Upon addition of cyclohexene to a solution of **1**, the absorption band at 940 nm due to **1** disappeared obeying a first-order kinetics (Figure 1a; see also Supporting

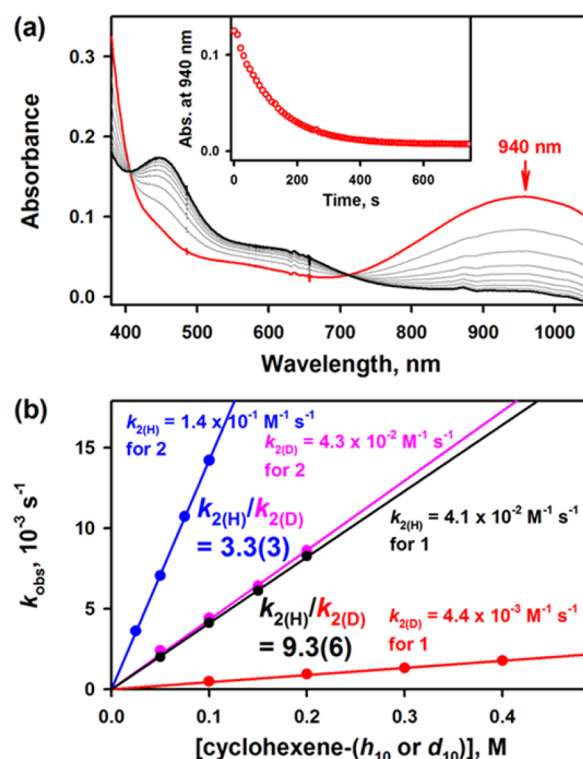


Figure 1. (a) UV-vis spectral changes observed in the reaction of **1** (0.50 mM, red line) and cyclohexene (0.20 M) in $CF_3CH_2OH-CH_3CN$ ($\nu/\nu = 1:1$) at 25 °C. Inset shows the time course monitored at 940 nm. (b) Plots of the first-order rate constant, k_{obs} (s^{-1}), against the concentration of cyclohexene (black for **1** and blue for **2**) and cyclohexene-*d*₁₀ (red for **1** and pink for **2**) to determine second-order rate constants, k_2 ($M^{-1} s^{-1}$) in the oxidation of cyclohexene and cyclohexene-*d*₁₀ by **1** and **2** in $CF_3CH_2OH-CH_3CN$ ($\nu/\nu = 1:1$) at 25 °C.

Information (SI), Figure S1 for the characterization of $Mn^{III}(N4Py)$ species as a product.¹² Pseudo-first-order rate constants increased linearly with an increase in the cyclohexene concentration (Figure 1b, black line), giving a second-order rate constant of $4.1 \times 10^{-2} M^{-1} s^{-1}$ at 25 °C (Table 1). Interestingly, when cyclohexene was replaced by cyclohexene-*d*₁₀, **1** decayed slowly, and the second-order rate constant was determined to be $4.4 \times 10^{-3} M^{-1} s^{-1}$ at 25 °C (Figure 1b, red line; Table 1). The rate of the cyclohexene-*d*₁₀ oxidation was

Table 1. Second-Order Rate Constants Obtained in the Oxidation of Cyclohexene, Cyclohexene- d_{10} , and Cyclooctene by 1, 2, 1-(HOTf) $_2$, and 2-(HOTf) $_2$ in CF $_3$ CH $_2$ OH–CH $_3$ CN ($\nu/\nu = 1:1$) at 25 °C


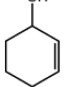
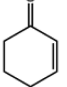
substrate	$k_2, M^{-1} s^{-1}$			
	1	2	1-(HOTf) $_2$	2-(HOTf) $_2$
cyclohexene	$4.1(2) \times 10^{-2}$	$1.4(1) \times 10^{-1}$	$4.5(2) \times 10^{-3}$	$4.2(2) \times 10^{-2}$
cyclohexene- d_{10}	$4.4(2) \times 10^{-3}$	$4.3(2) \times 10^{-2}$	$4.5(2) \times 10^{-3}$	$4.2(2) \times 10^{-2}$
cyclooctene	$5.4(3) \times 10^{-3}$	$3.2(2) \times 10^{-2}$	$3.2(2) \times 10^{-2}$	$1.1(1) \times 10^{-1}$

9.3(6) times slower than that of the cyclohexene oxidation (Figure 1b). In contrast to the formation of Mn^{III}(N4Py) species in the cyclohexene oxidation by 1 (vide supra), we observed the formation of Mn^{II}(N4Py) species in the oxidation of cyclohexene- d_{10} by 1 (Figure S2). Furthermore, when we determined the activation parameters for the oxidation of cyclohexene and cyclohexene- d_{10} by 1, the enthalpy values were the same but the entropies were different (Figure S3a; see the enthalpy (ΔH^\ddagger) and entropy (ΔS^\ddagger) values in the bottom of Figure S3).

In the oxidation of cyclohexene and cyclohexene- d_{10} by 2, we obtained second-order rate constants of 1.4×10^{-1} and $4.3 \times 10^{-2} M^{-1} s^{-1}$ at 25 °C, respectively (Figure 1b, blue and pink lines; Table 1; Figure S4 for UV–vis spectral changes), showing that the cyclohexene- d_{10} oxidation was 3.3(3) times slower than the cyclohexene oxidation. Thus, the present results indicate that the rates of the oxidation of cyclohexene and cyclohexene- d_{10} by Mn^{IV}O complexes depend on the allylic C–H(D) BDEs of the cyclohexene substrates. These results are in line with our previous results obtained in the oxidation of cyclohexene and cyclohexene- d_{10} by Fe^{IV}O(N4Py) and Ru^{IV}O(terpy)(bpm), in which the cyclohexene- d_{10} oxidation was slower than the cyclohexene oxidation with the rate ratios (i.e., $k_{2(H)}/k_{2(D)}$) of 55 and 38, respectively.¹⁰

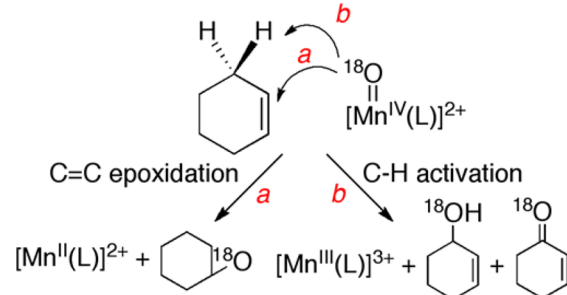
We then analyzed products formed in the oxidation of cyclohexene and cyclohexene- d_{10} by 1 and 2 under an Ar atmosphere. First, in the oxidation of cyclohexene and cyclohexene- d_{10} by 1 and 2, the product distributions were different depending on the Mn^{IV}O complexes and the substrates. As the results are shown in Table 2, the oxidation of cyclohexene by 1 afforded more allylic oxidation products (i.e., cyclohexenol and cyclohexenone) than epoxidation product (i.e., cyclohexene oxide). By carrying out an ^{18}O -

Table 2. Oxidation Products of Cyclohexene and Cyclohexene- d_{10} by 1 and 2^a

substrate	product yield (%)			
				
1	cyclohexene	6(3)	34(4)	6(3)
	cyclohexene- d_{10}	86(5)	3(1)	1(1)
2	cyclohexene	18(3)	26(3)	8(3)
	cyclohexene- d_{10}	84(6)	2(1)	trace

^aReactions were run with intermediates (1.0 mM) and substrates (50 mM) under an Ar atmosphere in CF $_3$ CH $_2$ OH–CH $_3$ CN ($\nu/\nu = 1:1$) at 25 °C. The product yield of “trace” is <0.5%.

labeled experiment with 1- ^{18}O , the oxygen atom in the oxygenated products was found to derive from the Mn^{IV}O complex (Scheme 2; Figure S5). In the oxidation of

Scheme 2. Products Formed in the C=C Double Bond Epoxidation (a) and the C–H Bond Activation (b) Reactions by Mn^{IV}–O Complexes

cyclohexene by 2, the amount of the cyclohexene oxide product was increased with the decrease of the cyclohexenol product, compared to the result obtained in the cyclohexene oxidation by 1 (Table 2). In contrast, the oxidation of cyclohexene- d_{10} by 1 and 2 yielded cyclohexene oxide predominantly (Table 2).

In the studies of Fe^{IV}O(N4Py) and Ru^{IV}O(terpy)(bpm), we have shown that the cyclohexene oxidation occurs exclusively via the C–H bond activation (Scheme 1A, pathway b), whereas the C=C double bond epoxidation is a viable pathway in the cyclohexene- d_{10} oxidation (Scheme 1A, pathway a), alongside the C–H bond activation.¹⁰ In the present case, the formation of the epoxide product is viable already with cyclohexene, but becomes totally dominant with cyclohexene- d_{10} . It should be noted that, in the oxidation of cyclohexene and cyclohexene- d_{10} by 1 and 2, the product distributions were quite consistent with their rate ratios ($k_{2(H)}/k_{2(D)}$ values) of 9.3(6) for 1 and 3.3(3) for 2, as the yield of cyclohexene oxide increased with the decrease of the rate ratio. On the basis of the results discussed above, we propose that the energy barriers of the C=C epoxidation and the C–H bond activation reactions by 1 and 2 are similar enough to produce both products on a sliding scale (vide infra). We also propose that the ratios of the reaction rates in the oxidation of cyclohexene versus cyclohexene- d_{10} by nonheme M^{IV}O complexes vary depending on the metal ions and the supporting ligands in metal catalysts, such as 9.3 for 1, 3.3 for 2, 55 for Fe^{IV}O(N4Py),^{10a} and 38 for Ru^{IV}O(terpy)(bpm).^{10b}

Chemoselectivity in the Oxidation of Cyclohexene by HOTf-Bound Mn^{IV}O Complexes. The oxidation of cyclohexene and cyclohexene- d_{10} by HOTf-bound Mn^{IV}O species, 1-(HOTf) $_2$ and 2-(HOTf) $_2$ (see the schematic drawing of 1-(HOTf) $_2$ and 2-(HOTf) $_2$ in Scheme 1, parts (D) and (E), respectively), was investigated. The protonated 1-(HOTf) $_2$ and 2-(HOTf) $_2$ complexes were prepared by literature

methods.^{4c} Upon addition of cyclohexene and cyclohexene-*d*₁₀ to the solution of 1-(HOTf)₂, the absorption band at 550 nm due to 1-(HOTf)₂ disappeared with the first-order decay profile (Figure 2a),¹⁴ resulting in the formation of Mn(II)

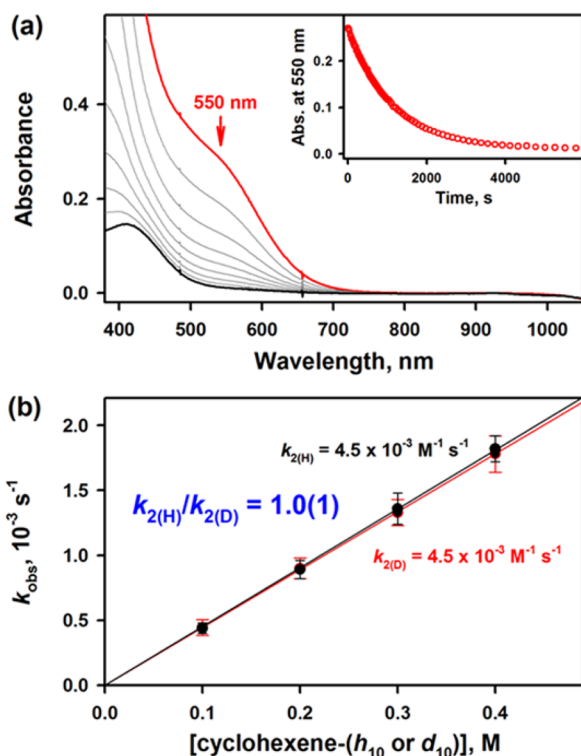
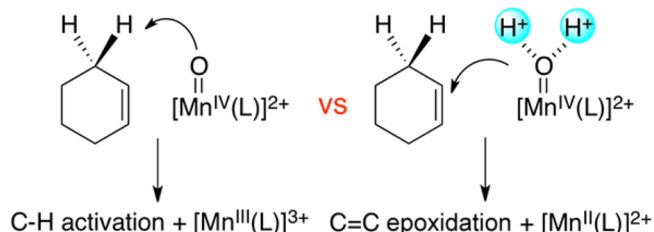


Figure 2. (a) UV-vis spectral changes observed in the reaction of 1-(HOTf)₂ (0.50 mM, red line) and cyclohexene (0.20 M) in CF₃CH₂OH-CH₃CN ($\nu/\nu = 1:1$) at 25 °C. Inset shows the time course monitored at 550 nm. (b) Plots of the first-order rate constant, k_{obs} (s⁻¹), against the concentration of cyclohexene-*h*₁₀ (black) and cyclohexene-*d*₁₀ (red) to determine second-order rate constants, k_2 (M⁻¹ s⁻¹), in the oxidation of cyclohexene-*h*₁₀ and cyclohexene-*d*₁₀ by 1-(HOTf)₂ in CF₃CH₂OH-CH₃CN ($\nu/\nu = 1:1$) at 25 °C.

species¹⁵ (Figure S6 for the characterization of the Mn^{II} product). Interestingly, the second-order rate constants determined in the oxidation of cyclohexene and cyclohexene-*d*₁₀ by 1-(HOTf)₂ were the same within the experimental error (Figure 2b; also see Table 2), indicating that the reaction rates are not affected by the C-H(D) BDEs of cyclohexene and cyclohexene-*d*₁₀. Similarly, upon addition of cyclohexene and cyclohexene-*d*₁₀ to the solution of 2-(HOTf)₂, the absorption band at 580 nm due to 2-(HOTf)₂ disappeared with the first-order decay profile (Figure S7a),¹⁴ and the second-order rate constant of $4.2 \times 10^{-2} \text{ M}^{-1} \text{ s}^{-1}$ was determined in the reactions of cyclohexene and cyclohexene-*d*₁₀ (Table 1; Figure S7b), indicating again that the C-H(D) BDEs of cyclohexene and cyclohexene-*d*₁₀ do not affect the reaction rates. These results are different from those observed in the oxidation of cyclohexene and cyclohexene-*d*₁₀ by 1 and 2 in the absence of protons, in which the reaction rates were different depending on the allylic C-H(D) BDEs of the olefin substrates (Figure 1b; also see Scheme 2). Further, when we determined the activation parameters in the oxidation of cyclohexene and cyclohexene-*d*₁₀ by 1-(HOTf)₂, the enthalpy and entropy values were also the same (Figure S3b; see the enthalpy (ΔH^\ddagger) and entropy (ΔS^\ddagger) values in Figure S3). Thus, different from

the mechanisms proposed in the oxidation of cyclohexene and cyclohexene-*d*₁₀ by 1 and 2 (Scheme 2, reaction pathways *a* and *b*), the oxidation of cyclohexene and cyclohexene-*d*₁₀ by 1-(HOTf)₂ and 2-(HOTf)₂ occurs only via the C=C epoxidation pathway (Scheme 3). In addition, it is notable

Scheme 3. Preferred Reaction Pathways in the Oxidation of Cyclohexene by Mn^{IV}O and Protonated Mn^{IV}O Species



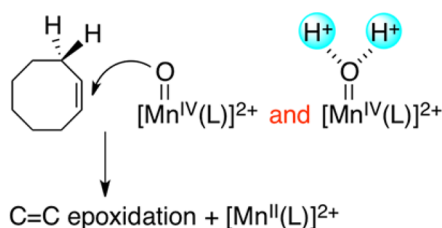
that the reactions of the HOTf-bound Mn^{IV}O complexes, 1-(HOTf)₂ and 2-(HOTf)₂, were slower than those of 1 and 2 in case of the cyclohexene substrate, but nearly the same with cyclohexene-*d*₁₀ (Table 1).

Then, why are the mechanisms in the oxidation of cyclohexene by Mn^{IV}O complexes and their HOTf-bound Mn^{IV}O complexes different (e.g., the dominant C-H hydroxylation by 1 and the C=C epoxidation by 1-(HOTf)₂ in Scheme 3)? Also, why are the reaction rates in the oxidation of cyclohexene and cyclohexene-*d*₁₀ by Mn^{IV}O complexes and their HOTf-bound Mn^{IV}O complexes different (e.g., the oxidation of cyclohexene by 1 ($k_2 = 4.1 \times 10^{-2} \text{ M}^{-1} \text{ s}^{-1}$) is faster than that by 1-(HOTf)₂ ($k_2 = 4.5 \times 10^{-3} \text{ M}^{-1} \text{ s}^{-1}$), as shown in Table 1)? As we have suggested previously,^{4c} the binding of Brønsted acid by Mn^{IV}O species may cause a steric hindrance that interrupts the approach of substrate to the Mn-O moiety, resulting in the decrease of reaction rates in the HOTf-bound Mn^{IV}O complexes, 1-(HOTf)₂ and 2-(HOTf)₂. In addition, the reactivity toward H atom abstraction involving 1s orbital may be more diminished due to the more severe steric hindrance, compared to the approach of the HOTf-bound Mn^{IV}O complexes toward the double bond epoxidation involving 2 π orbital. Therefore, the reaction pathway is altered to the C=C epoxidation pathway in the oxidation of cyclohexene by the HOTf-bound Mn-O moiety in 1-(HOTf)₂ and 2-(HOTf)₂ from the C-H bond activation by the Mn-O moiety in 1 and 2 (see Scheme 3). Because the oxidation potential of cyclohexene (2.30 V vs SCE)^{3c} is significantly higher than the reduction potential of 1-(HOTf)₂ (1.65 V vs SCE),^{4c} electron transfer from cyclohexene to 1-(HOTf)₂ is thermodynamically infeasible. In such a case, the rate constant of epoxidation of cyclohexene-*d*₁₀ by 1 is not altered by binding of HOTf to 1 (Table 1). In this section, we have shown that the protonated Mn^{IV}O complexes favor the C=C double bond epoxidation over the allylic C-H bond activation in the cyclohexene oxidation reactions. The change of the chemoselectivity in the cyclohexene oxidation was rationalized with a steric hindrance caused by protonation of the Mn-O moiety.

Chemoselectivity in the Oxidation of Cyclooctene by Mn^{IV}(O) and HOTf-Bound Mn^{IV}O Complexes. The cyclooctene oxidation by [Mn^{IV}(O)(N4Py)]²⁺ (1) and [Mn^{IV}(O)(Bn-TPEN)]²⁺ (2) was investigated to confirm the effect of the allylic C-H BDEs of olefins on the C-H bond activation versus the C=C double bond epoxidation, since the BDE of

cyclooctene (85 kcal mol⁻¹) is greater than that of cyclohexene (81 kcal mol⁻¹).¹⁶ Upon addition of cyclooctene to the solutions of **1** and **2**, the Mn^{IV}O complexes decayed with a pseudo-first-order decay profile (Figure S8). Pseudo-first-order rate constants, determined by the first-order fitting of the kinetic data for the decay of **1** and **2**, increased linearly with the increase of the cyclooctene concentration (Figure S9), giving second-order rate constants of $5.4 \times 10^{-3} \text{ M}^{-1} \text{ s}^{-1}$ for **1** and $3.2 \times 10^{-2} \text{ M}^{-1} \text{ s}^{-1}$ for **2** at 25 °C (Table 1). We also found that cyclooctene oxide was the sole product with the yields of 91(5)% for **1** and 94(3)% for **2**, indicating that the oxidation of cyclooctene by Mn^{IV}O complexes occurs via the C=C double bond epoxidation (Scheme 4). When the cyclooctene oxidation

Scheme 4. Preferred Reaction Pathway in the Oxidation of Cyclooctene by Mn^{IV}O and HOTf-bound Mn^{IV}O Species



was carried out with I-¹⁸O, the oxygen atom in the cyclooctene oxide product was found to derive from the Mn^{IV}O complex (Figure S10). Further, the manganese products formed in the oxidation of cyclooctene by **1** and **2** were determined to be manganese(II) species, based on the EPR and ESI-MS analysis of the reaction solutions (Figures S11 and S12). These results demonstrate that the cyclooctene oxidation by **1** and **2** occurs only via the C=C double bond epoxidation to give the epoxide and Mn^{II} products (Scheme 4), which is different from the oxidation of cyclohexene by the Mn^{IV}O complexes (Scheme 3).

The oxidation of cyclooctene by the HOTf-bound Mn^{IV}O complexes, **1**-(HOTf)₂ and **2**-(HOTf)₂, was also investigated. Upon addition of cyclooctene to the solutions of **1**-(HOTf)₂ and **2**-(HOTf)₂, the HOTf-bound Mn^{IV}O complexes disappeared with the first-order decay profile (Figure S13),¹⁴ affording the formation of Mn(II) species (Figure S14 for the analysis of the Mn^{II} products). In these reactions, cyclooctene oxide was the product with the yields of 95(4)% for **1**-(HOTf)₂ and 96(4)% for **2**-(HOTf)₂, indicating that the oxidation of cyclooctene by the HOTf-bound Mn^{IV}O complexes occurs via the C=C double bond epoxidation (Scheme 4). The second-order rate constants were determined to be $3.2 \times 10^{-2} \text{ M}^{-1} \text{ s}^{-1}$ for **1**-(HOTf)₂ and $1.1 \times 10^{-1} \text{ M}^{-1} \text{ s}^{-1}$ for **2**-(HOTf)₂ at 25 °C (Table 1; Figure S15). It is of interest to note that the rates of the cyclooctene oxidation increased by protonating the Mn—O moiety, which is different from the case of the cyclohexene oxidation by **1**-(HOTf)₂ and **2**-(HOTf)₂ (vide supra). For example, the rates of **1**-(HOTf)₂ and **2**-(HOTf)₂ were ~10 times slower than those of **1** and **2** in the cyclohexene oxidation, whereas the rates of **1**-(HOTf)₂ and **2**-(HOTf)₂ were ~5 times faster than those of **1** and **2** in the cyclooctene oxidation (see Table 1). We rationalize the increase of the reaction rates in the oxidation of cyclooctene by the HOTf-bound Mn^{IV}O complexes by the involvement of ET in the cyclooctene epoxidation reaction due to the lower ionization potential of cyclooctene (8.98 eV) as compared with that of cyclohexene (9.12 eV).¹⁷ In contrast to

the oxidation of cyclohexene by the HOTf-bound Mn^{IV}O complexes, **1**-(HOTf)₂ and **2**-(HOTf)₂, which is susceptible to the steric effects of HOTf bound to the oxo group (vide supra), the ET pathway in the cyclooctene oxidation enhanced by the protonation of the Mn^{IV}O complexes is insensitive to the steric effects, because ET requires little interaction between reactants. However, more detailed mechanistic studies are required to delineate the involvement of ET in the epoxidation of cyclooctene by the HOTf-bound Mn^{IV}O complexes, **1**-(HOTf)₂ and **2**-(HOTf)₂.¹⁸ In this section, we have shown that the oxidation of cyclooctene by Mn^{IV}O and HOTf-bound Mn^{IV}O complexes occurs only via the C=C double bond epoxidation pathway due to the high allylic C—H BDE of cyclooctene (Scheme 4). Thus, as shown in the oxidation of cyclohexene-*d*₁₀ by Mn^{IV}O complexes (vide supra), the allylic C—H bond strength of cyclic olefins is another factor that determines the chemoselectivity (e.g., C—H bond activation versus C=C double bond epoxidation) in the oxidation of cyclic olefins by mononuclear nonheme metal-oxo species.

Density Functional Theory (DFT) Calculations. DFT calculations were performed to investigate the mechanistic details on the C—H bond activation versus the C=C double bond epoxidation with cyclohexene and cyclooctene as substrates (see SI, Density Function Theory Section; Tables S1–S15). As described by the experiments detailed above, there are both hydroxylation and epoxidation products present in various degrees, that turns into exclusively epoxidation products upon deuteration when using cyclohexene. This indicates that the energetic difference in the rate limiting steps between hydroxylation and epoxidation reactions are small enough to be influenced by small changes in the substrate, catalyst, and/or environment. In terms of energies, the difference should be within few kcal mol⁻¹. Therefore, if the calculations are reliable, we can expect the calculations to show similar barrier heights for cyclohexene, quite possibly within accepted error margins, rather than a clear preference for one pathway or another.

In previous theoretical and experimental studies, the ground state of **1** was shown to be an $S = 3/2$ state.¹⁹ Three possible reaction pathways were found for this spin state: the so-called π -channel by abstracting a β -electron from the substrate to the π^*_{xz} -orbital, the σ -channel where an α -electron is abstracted to the $\sigma^*_{z^2}$ orbital,^{19b} and the excited state reactivity (ESR) pathway. In the latter pathway, an electron is excited to a higher orbital ($\pi^*_{xz} \rightarrow \sigma^*_{xy}$) at an affordable energetic cost, followed by an α -electron abstraction to the empty π^*_{xz} . This excited state configuration was shown to be connected to the lowest transition states in C—H bond activations¹⁹ as well as in sulfoxidation reactions.^{19b} This ESR is very specific for manganese and has not been observed in any other comparable metal-oxo species. Figure 3 details schematically the electron transfer diagrams of these three reactions. Together with the $S = 1/2$ and $S = 5/2$ states, there are thus five different electron transfer variations that need to be explored in each of the reactions for a proper theoretical treatment. Noteworthy is that the $S = 3/2$ π -pathway is not even connected to the preferred electron configuration at the intermediate stage (the spin state of the resulting Mn^{III}OH moiety is $S = 1$ instead of preferred $S = 2$).

In line with this, we indeed found five electronically different pathways for the cyclohexene C—H bond activation reaction by **1**. The $S = 3/2$ ground state configuration (Figure 4a, blue and green) is 0.3 and 0.5 kcal mol⁻¹ higher than the sum of **1**

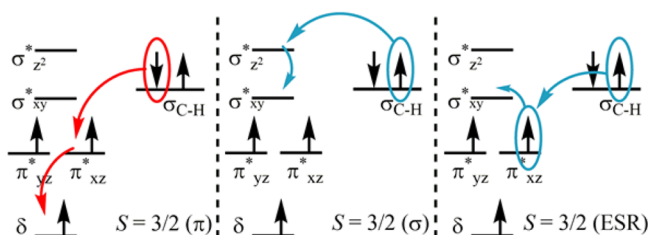


Figure 3. Three different pathways for electron transfer to **1** in the $S = 3/2$ state. Utilizing the so-called π -channel (π), a β -electron from the substrate is transferred to π^{*}_{xz} orbital. A second step is required where the electron is relaxed down to the δ orbital, possibly without any energy barrier. Similarly, the σ -channel (σ) transferring an α -electron to $\sigma^{*}_{z^2}$ also requires a second step to transfer the electron to σ^{*}_{xy} . The excited state reactivity pathway (ESR) in contrast initially excites an electron to the σ^{*}_{xy} orbital, and an α -electron can be transferred to the empty π^{*}_{xz} orbital at a moderate energetic cost.

and cyclohexene noninteracting energies together (which is set as the $\Delta E = 0$ point). The difference between these two structures reflects a slightly different mode of binding by the substrate, depending on the ensuing pathway. These state gives rise to high transition state (TS) energies at 24.3 and 25.5 kcal mol⁻¹ (TS_H), depending on the pathway (π or σ). As noted before,¹⁹ the reactant complex R_c of the ESR pathway is very unstable and difficult to obtain even theoretically,^{19b} but can occasionally be stabilized when a substrate is present.^{19a} We found this state to be at 17.8 kcal mol⁻¹ (Figure 4a, red). A very small geometry perturbation allows it to reach TS_H at 17.9 kcal mol⁻¹. This ESR leads directly to the preferred electron configuration at the intermediate stage (I_c).

Given the role of ESR in the reaction, we sought out the minimum energy crossing point (MECP) between the $S = 3/2$ π and ESR pathways. An MECP structure was found geometrically close to TS_H for the excited state (Figure 4a and Table S12), and the energy was at 16.8 kcal mol⁻¹. To verify the two-spin state nature of this MECP, its geometry was used as a starting point for optimization. Using the wave function corresponding to the ground state, the optimization

yielded the ground state R_c. Using the excited state wave function, however, the optimization went to I_c. Hence, this MECP may act as an effective TS.

While the $S = 1/2$ state also features a low-energy pathway (Figure 4a, black), we deem this reaction less likely as an electron shift as well as a spin flip has to occur before the reaction ($\pi^{*}_{xz}(\alpha) \rightarrow \delta(\beta)$) to reach the $S = 1/2$ state. While this may be feasible, the reaction again has to switch spin states and orbitals after the reaction, to access the lower energy $S = 3/2$ or $5/2$ states at I_c. This flip-flopping and orbital shifting of electrons seem to be very unnecessary, compared to a simple electron excitation at $S = 3/2$ (ESR) that will lead directly to the desired intermediate state. Similarly, the $S = 5/2$ state leads directly to the same preferred electronic configuration at I_c as the $S = 3/2$ ESR pathway, except for the spin type at the substrate carbon radical (C•; α instead of β). However, due to its high energy at the beginning of the reaction (33.9 kcal mol⁻¹) as well as in the MECP area (Figure 4a gray, the potential energy surface shape obtained by constrained optimizations), in combination with a required spin flip, this spin state does not seem to offer any particular advantage compared to the $S = 3/2$ ESR pathway.

To compare the calculated values to the experimental rates, we divide the experimentally obtained rate (4.1×10^{-2} M⁻¹ s⁻¹) by 2, accounting for the presence of two equivalent protons available in cyclohexene for C—H bond activation.²⁰ Subsequent use of the Eyring equation at 25 °C yields in an energy barrier of 19.7 kcal mol⁻¹. This value is within reasonable error margins from the $S = 1/2$ state and the ESR barrier, as well as the MECP value (18.9, 17.9, and 16.8 kcal mol⁻¹, respectively). Hence, the experimental value largely confirms that all of the calculated pathways are possible, and does not specifically distinguish a pathway over another.

The C—H activation pattern found for cyclooctene is similar to cyclohexene, except for the absolute numbers (Figure 4b). The stronger C—H bond lead to higher energy barriers than for cyclohexene, as expected. The $S = 3/2$ ESR pathway was also found to have the lowest energy barrier at 20.1 kcal mol⁻¹. Unlike cyclohexene, however, the MECP area is before all the

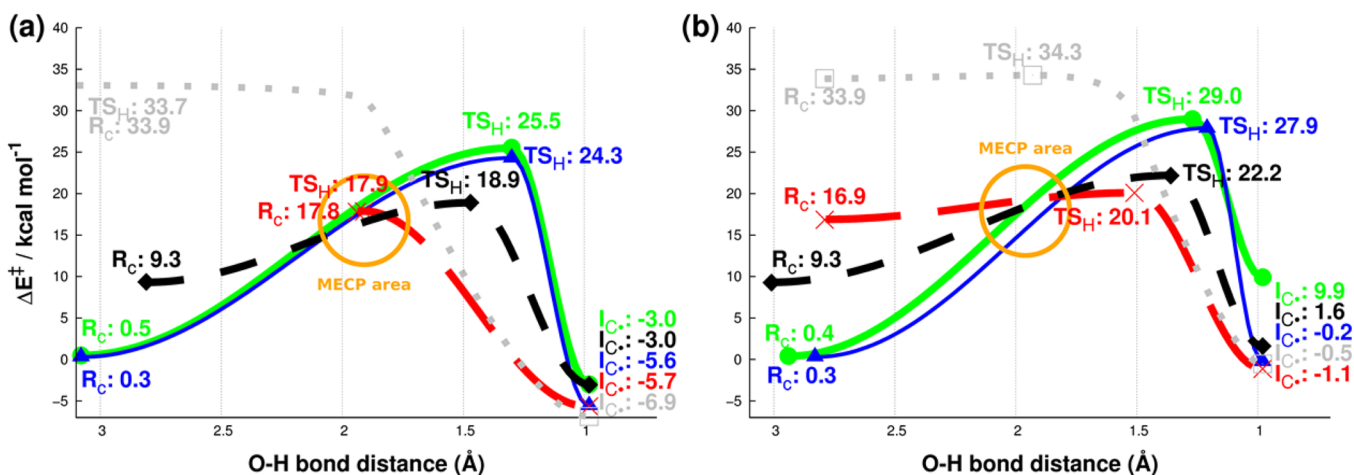


Figure 4. DFT-calculated energy profile of H atom abstraction reaction of (a) cyclohexene and (b) cyclooctene by **1**. The reference state (0 kcal/mol) is taken as the sum of the energies of noninteracting **1** and substrate. The reaction coordinate is taken as the forming O—H bond distance. An MECP between $S = 3/2$ π and ESR states was found in the marked area. The exact graph values are shown in Tables S2, S4, S12, and S14. The connecting sinusoidal lines between the data points are mostly generic, but the approximate shape of the $S = 5/2$ pathway was confirmed by constrained optimizations. See text for descriptions of the different states. R_c = reactant complex, TS_H = H atom abstraction TS, and I_c = substrate radical intermediate. The spin state surfaces are $S = 1/2$ (black, \blacklozenge), $3/2$ π (green, \bullet), $3/2$ σ (blue, \blacktriangle), $3/2$ ESR (red, \times), and $5/2$ (gray, \square).

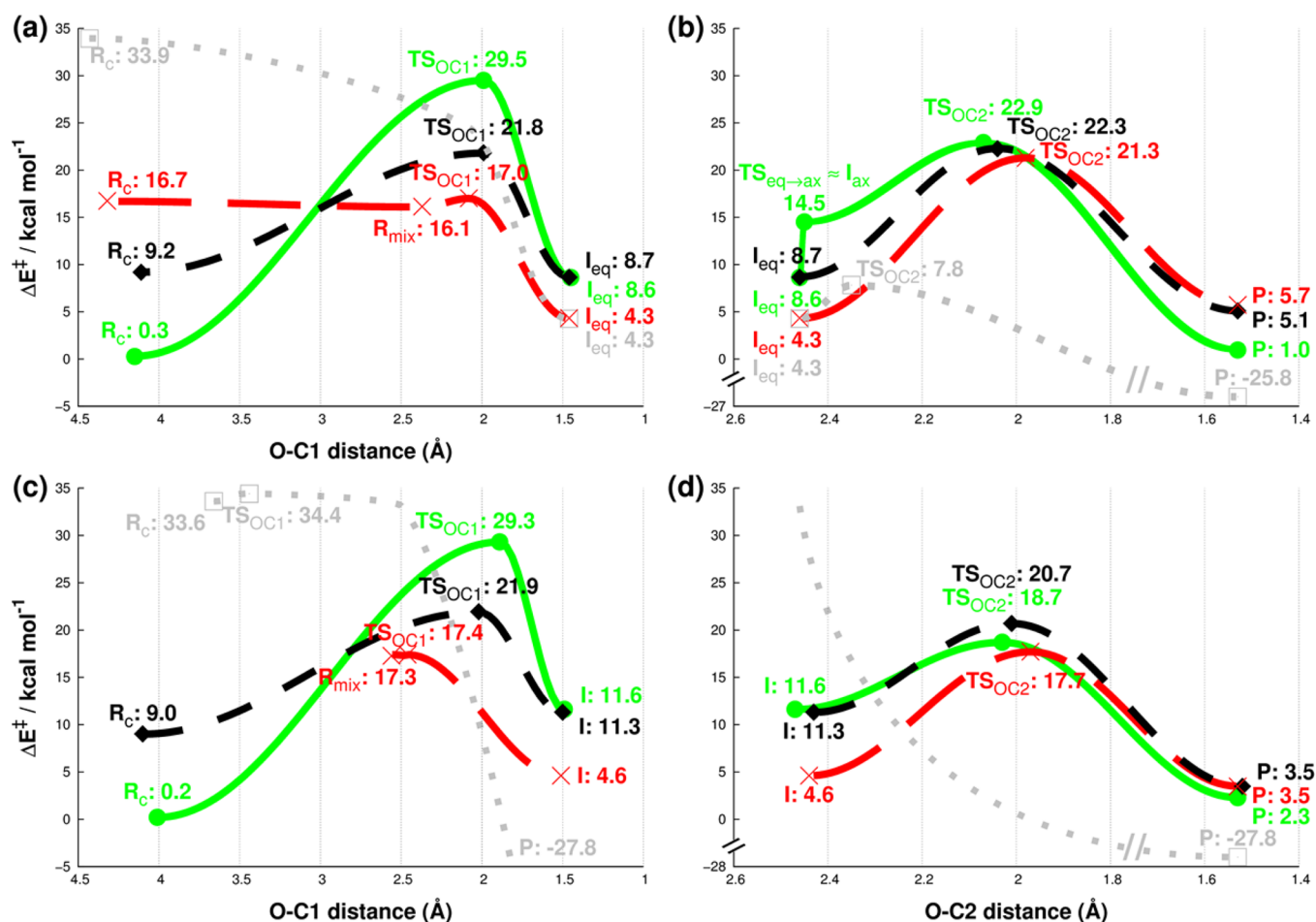


Figure 5. DFT-calculated energy profiles of the cyclohexene (a and b) and cyclooctene (c and d) epoxidation reactions by **1**. The first part of the reaction is described by (a and c), where the reaction coordinate is the oxygen atomic distance to the first bond forming carbon atom in the substrate (O—C1). The second part (b and d) uses the second bond formation (O—C2) as the reaction coordinate. The exact graph values are shown in Tables S3, S5, S13, and S15. R_c = reactant complex, R_{mix} = reactant with partial radical on substrate, TS_{OC1} = first O—C bond formation TS, I_{eq} = equatorial O—C1 bond intermediate, $TS_{eq \rightarrow ax}$ = axial to equatorial O—C1 bond TS, I_{ax} = axial O—C1 bond intermediate, TS_{OC2} = second O—C bond formation (O—C2) TS and P = epoxidated product. $TS_{eq \rightarrow ax}$ and I_{ax} occupy the same point within the resolution of this graph. The spin state surfaces are $S = 1/2$ (black, \blacklozenge), $3/2 \pi$ (green, \bullet), $3/2$ ESR (red, \times), and $5/2$ (gray, \square).

transition states. Thus, while the electron configurations can change at MECP (found at 17.9 kcal mol⁻¹), the reaction would still have to cross a proper transition state, the lowest being 20.1 kcal mol⁻¹.

The first step of the epoxidation reaction of cyclohexene involves forming an O—C bond to one of the cyclohexene double bond carbons, C1 (Figure 5a). The forming O—C1 bond is approximately parallel (equatorial) to the substrate plane (Table S13), with the substrate ring being in a “chair” conformation. This occurs through TS_{OC1} , leading to intermediate I_{eq} . In the case of the $S = 3/2 \pi$ pathway, the reaction has a high energy barrier, 29.5 kcal mol⁻¹ (Figure 5a, green). Despite an extensive search, no σ pathway was found here. A viable pathway is again given by ESR. An initial interaction between **1** in the excited $S = 3/2$ state and the substrate causes a partial electron donation from the substrate to form a mixed radical reactant (R_{mix}) at 16.1 kcal mol⁻¹ (Figure 5a, red), with about 0.3 in spin on the substrate (Table S8). This ESR has a TS_{OC1} at 17.0 kcal mol⁻¹, which is substantially lower than the next higher TS_{OC1} (21.8 kcal mol⁻¹ in $S = 1/2$; Figure 5a, black). However, despite trials, we were unable to find an MECP for the two $S = 3/2$ states along the epoxidation reaction pathway. Furthermore, due to the high

energy of the $S = 5/2$ state at R_c (33.9 kcal mol⁻¹), we deem this state to be unlikely to play a role in this part of the reaction, also confirmed by the high energy obtained with constrained optimizations (Figure 5b, gray).

The second O—C bond formation, O—C2 (Figure 5b), features a change of the substrate “chair” formation (I_{eq}) to a “boat” configuration (I_{ax}). This causes the O—C1 bond to become approximately perpendicular (axial) to the substrate plane (Table S13). Albeit a stable I_{ax} structure was found only in the ground state $S = 3/2$ configuration (Figure 5b, green), the O—C1 bond is clearly of axial type in all the configurations at the O—C2 bond formation TS stage, TS_{OC2} (Table S13). Regardless, it is clear that only the $S = 5/2$ state would have any chance to perform this reaction (Figure 5b, gray, $TS_{OC2} = 7.8$ kcal mol⁻¹) as any other configurations, including the $S = 3/2$ ESR, have too high barriers for this reaction. In fact, these high barriers would have made this step become the rate limiting step for the $S = 1/2$ and the $S = 3/2$ ESR (Figure 5b, black for $S = 1/2$ and red for $S = 3/2$ ESR). Hence, it seems like a spin flip has to occur somewhere along the reaction, especially since the product Mn^{II} (**P**) is found in its high spin state (−25.8 kcal mol⁻¹). Considering the tremendously low TS_{OC2} , a spin flip before TS_{OC2} seems therefore very likely.

A similar picture emerges from the epoxidation reaction with cyclooctene. The $S = 3/2$ ESR has the lowest transition state in the first part of the reaction (Figure 5c). A notable difference here is that the $S = 5/2$ state, when past the transition state, forms the product directly. Constrained optimization however indicates that the $S = 5/2$ energy is high at the O—C1 distance corresponding to TS_{OC1} for the $S = 3/2$ ESR state. Hence, the likely scenario here is again that the reaction utilizes $S = 3/2$ ESR for the first half of the reaction, and then switches to $S = 5/2$ at the intermediate (I) state to perform the rest of the reaction without barriers (Figure 5d).

What is then the prediction from DFT regarding the choice of reaction pathway? For cyclohexene, the lowest effective TS is at MECP with 16.8 kcal mol⁻¹ in barrier; hence, an H atom abstraction is a real possibility, consistent with the experimental results. Looking at the obtained results in perspective, however, the DFT results show that H atom abstraction and epoxidation reactions face similar rate-limiting barriers within calculation error margins (ESR epoxidation: 17.0 kcal mol⁻¹ and the effective TS at MECP: 16.8 kcal mol⁻¹). It is therefore not easy to pinpoint a particular pathway preference with clear certainty. This uncertainty, however, is still informative and fits our predictions (vide supra). We can conclude that the close energy barriers are consistent with experiments that yield both epoxidation and hydroxylation products depending on the precise experimental conditions, which require very close competing rate-limiting barriers. The fact that the product distribution changes with a minimal system change, such as supporting ligand, metal ion, deuterium substitution in olefin C—H bond, or presence of protons, further confirms this view, and is akin to what had been already seen in the Fe^{IV}O and Ru^{IV}O cases.¹⁰ The situation is slightly more definite for cyclooctene, where the epoxidation rate-limiting barrier (ESR 17.4 kcal mol⁻¹) is clearly lower than the H atom abstraction barrier (ESR: 20.1 kcal mol⁻¹), and is largely in accord with the experimental results, which show preference for the epoxidation reaction.

Finally, it is quite possible to refine the results further by calculating the free energies, including tunneling,²¹ to the cost of introducing larger error margins (see the SI, DFT section for a discussion). This approach led in the case of Fe^{IV}O to energy barriers that matched the experiments perfectly.^{10a} However, this will inevitably also lead to questions about calculation accuracies, as we are merely adjusting the values within the accepted error margins, without really increasing our overall insight into the reactivity of the current system. Our discussion here is based on the electronic energy, which incidentally matches the experimental results very well, which has also been our general experience so far.¹⁸

CONCLUSION

The mechanisms of the oxidation of olefins by mononuclear nonheme metal-oxo complexes have been explored less clearly, but are started being investigated recently using spectroscopically well-characterized synthetic nonheme metal-oxo complexes.¹⁰ In the present study, we have shown for the first time that the oxidation of cyclic olefins by mononuclear nonheme Mn^{IV}O and HOTf-bound Mn^{IV}O complexes can occur via the allylic C—H bond activation or C=C double bond epoxidation mechanisms, depending on the chemical property of the Mn^{IV}O species, such as the supporting ligands and the binding of protons at the Mn^{IV}=O moiety, and the olefin substrates (i.e., the allylic C—H(D) BDEs of olefins). DFT

calculations confirm the view that the energy barriers are similar for the both pathways (with a slight preference for C—H activation) for cyclohexene, while epoxidation is preferred for cyclooctene. The calculations also show possibilities of ESR as well as multistate reactivity in this system, and that in the case of cyclohexene, MECP can act as an effective transition state.

EXPERIMENTAL SECTION

Materials. Commercially available chemicals were used without further purification unless otherwise indicated. Solvents were dried according to the known procedures and distilled under an Ar atmosphere prior to use.²² Trifluoromethanesulfonic acid (HOTf, OTf = CF₃SO₃⁻) was purchased from Aldrich Chemicals and used as received. H₂¹⁸O (95% ¹⁸O-enriched) was purchased from ICON Services Inc. (summit, NJ, U.S.A.). Iodosylbenzene (PhIO), N4Py and Bn-TPEN ligands, and Mn^{II}(OTf)₂·2CH₃CN were prepared by literature methods.^{23–25} [Mn^{II}(L)]²⁺ and [Mn^{IV}(O)(L)]²⁺ (L = N4Py and Bn-TPEN) were prepared by literature methods.^{4,12,26} Mononuclear Mn^{IV}(O) complexes, [Mn^{IV}(O)(N4Py)]²⁺ (1) and [Mn^{IV}(O)(Bn-TPEN)]²⁺ (2), were generated by reacting [Mn^{II}(N4Py)]²⁺ and [Mn^{II}(Bn-TPEN)]²⁺ with iodosylbenzene (PhIO; 4.0 equiv) in CF₃CH₂OH/CH₃CN ($\nu/\nu = 1:1$) at 25 °C, respectively.^{4,12,24} The HOTf-bound Mn(IV)-oxo complexes, 1-(HOTf)₂ and 2-(HOTf)₂, were generated by adding HOTf (50 mM) into the solution of in situ generated 1 and 2 in CF₃CH₂OH/CH₃CN ($\nu/\nu = 1:1$) at 25 °C, respectively, as reported previously.^{4c} Addition of HOTf to an in situ generated solution of 1 in CF₃CH₂OH—CH₃CN ($\nu/\nu = 1:1$) at 25 °C afforded a reddish brown solution and resulted in the disappearance of the absorption band at 940 nm due to 1, accompanied by a new absorption band formation at 550 nm due to 1-(HOTf)₂. Similar spectral changes were also obtained for 2; the absorption band at 1020 nm due to 2 disappeared with the appearance of an absorption band at 580 nm due to 2-(HOTf)₂.

Instrumentation. UV–vis spectra were recorded on a Hewlett-Packard 8453 diode array spectrophotometer equipped with a UNISOKU Scientific Instruments Cryostat USP-203A for low-temperature experiments or on a UNISOKU RSP-601 stopped-flow spectrometer equipped with a MOS-type highly sensitive photodiode-array. Electrospray ionization mass spectra (ESI MS) were collected on a Thermo Finnigan (San Jose, CA, U.S.A.) LCQ Advantage MAX quadrupole ion trap instrument, by infusing samples directly into the source using a manual method. X-band EPR spectra were recorded at 5 K using X-band Bruker EMX-plus spectrometer equipped with a dual mode cavity (ER 4116DM). Low temperature was achieved and controlled with an Oxford Instruments ESR900 liquid He quartz cryostat with an Oxford Instruments ITC503 temperature and gas flow controller. The experimental parameters for EPR measurement were as follows: Microwave frequency = 9.647 GHz, microwave power = 1.0 mW, modulation amplitude = 10 G, gain = 1.0 × 10⁴, modulation frequency = 100 kHz, time constant = 40.96 ms, and conversion time = 81.00 ms. Product analysis for oxidation reactions was performed with an Agilent Technologies 6890N gas chromatograph (GC) and a Thermo Finnigan (Austin, Texas, U.S.A.) FOCUS DSQ (dual stage quadrupole) mass spectrometer interfaced with Finnigan FOCUS gas chromatograph (GC-MS).

Kinetic Measurements. All reactions were run in a 1 cm UV cuvette by monitoring UV–vis spectral changes of reaction solutions. First-order rate constants were determined under pseudo-first-order conditions (e.g., [substrate]/[1] > 10) by fitting the changes in absorbance for the decay of peaks due to Mn^{IV}(O) intermediates in the oxidation reactions of substrates (5.0 × 10⁻² to 0.50 M) by [Mn^{IV}(O)(N4Py)]²⁺ (1), [Mn^{IV}(O)(Bn-TPEN)]²⁺ (2), 1-(HOTf)₂, and 2-(HOTf)₂ in CF₃CH₂OH/CH₃CN ($\nu/\nu = 1:1$) at 25 °C. Reactions of 1, 2, 1-(HOTf)₂, and 2-(HOTf)₂ with substrates were monitored by the changes in the absorption band at 940 nm for 1, 1020 nm for 2, 550 nm for 1-(HOTf)₂, and 580 nm for 2-(HOTf)₂. The first-order plots were linear for three or more half-lives with the correlation coefficient of $\rho > 0.99$. In each case, it was confirmed that

the rate constants derived from at least five independent measurements agreed within an experimental error of $\pm 5\%$. The pseudo-first-order rate constants increased proportionally with the concentrations of substrates, from which second-order rate constants were determined. The kinetic experiments were run at least in triplicate, and the data reported represent the average of these reactions.

Product Analysis. Products formed in the oxidation of cyclohexene, cyclohexene- d_{10} , and cyclooctene by **1** and **2** under an Ar atmosphere were analyzed by GC and/or GC-MS. Quantitative analysis was performed by comparing the ratio of peak areas of products and internal standard (i.e., decane) with those of authentic samples and internal standard. In the oxidation of cyclohexene by **1** and **2**, GC and GC-MS were used to analyze products. Cyclohexenol (34(3)%), cyclohexenone (6(1)%), and cyclohexene oxide (8(1)%) were obtained as products in the oxidation of cyclohexene (0.20 M) by **1** (0.50 mM). Similarly, cyclohexenol (26(3)%), cyclohexenone (8(2)%), and cyclohexene oxide (18(2)%) were obtained as products in the oxidation of cyclohexene (0.20 M) by **2** (0.50 mM). However, cyclohexene- d_{10} oxide with the yields of 86(5)% for **1** and 84(6)% for **2** was obtained as a sole product in the oxidation of cyclohexene- d_{10} by **1** and **2** under an Ar atmosphere in $\text{CF}_3\text{CH}_2\text{OH}/\text{CH}_3\text{CN}$ ($\nu/\nu = 1:1$) at 25 °C (see Table 2). When the reactions were performed with ^{18}O -labeled **1** ($1\text{-}^{18}\text{O}$), we found that oxygens in the cyclohexenol, cyclohexenone, and cyclohexene oxide derived from **1** (Figure S5). In the oxidation of cyclooctene by **1** and **2**, cyclooctene oxide with the yields of 91(5)% for **1** and 94(3)% for **2** was obtained as a sole product under an Ar atmosphere in $\text{CF}_3\text{CH}_2\text{OH}/\text{CH}_3\text{CN}$ ($\nu/\nu = 1:1$) at 25 °C. When this reaction was performed with ^{18}O -labeled **1** ($1\text{-}^{18}\text{O}$), we found that oxygen in cyclooctene oxide derived from **1** (Figure S10). Similarly, in the oxidation of cyclooctene by 1-(HOTf)_2 and 2-(HOTf)_2 , cyclooctene oxide with yields of 95(4)% for 1-(HOTf)_2 and 96(4)% for 2-(HOTf)_2 was also obtained as a sole product under an Ar atmosphere in $\text{CF}_3\text{CH}_2\text{OH}/\text{CH}_3\text{CN}$ ($\nu/\nu = 1:1$) at 25 °C.

DFT Calculations. Density functional theory (DFT)²⁷ calculations were performed using the B3LYP functional²⁸ as implemented in the Gaussian 09 (G09) package.²⁹ The geometries were optimized using the LACVP basis set, which uses Los Alamos ECP on transition metals³⁰ (slightly tweaked as implemented in the Jaguar program³¹), and 6-31G on the rest of the atoms.³² The stationary points were confirmed by frequency calculations, and the transition states were connected with the ground states on both sides by performing IRC calculations and continuing relaxing the geometry down to the ground state from the end geometry obtained by IRC. The high molecular charge (2^+) made it necessary to perform the optimizations in solvent to avoid artificial results (see the SI for Free Energy Calculations).³³ Solvent (acetonitrile) effects were included using CPCM model³⁴ with UFF cavity, per G09 default. Single-point energy evaluations on the optimized geometry were done with the Def2-TZVPP basis set.³⁵ This resulting electronic energy (ΔE) was used throughout the text as the final energy due to sufficient accuracy (see SI for Free Energy Calculations). MECP was found using a shell program to G09 that iterates to the same energy and geometry for two different electron configurations.³⁶

■ ASSOCIATED CONTENT

● Supporting Information

The Supporting Information is available free of charge on the ACS Publications website at DOI: 10.1021/jacs.6b06252.

Figures S1–S16, Tables S1–S15, and DFT calculation section with DFT coordinates (PDF)

■ AUTHOR INFORMATION

Corresponding Authors

*fukuzumi@chem.eng.osaka-u.ac.jp

*wnnam@ewha.ac.kr

Author Contributions

[§]These authors contributed equally to this work.

Notes

The authors declare no competing financial interest.

■ ACKNOWLEDGMENTS

The authors acknowledge financial support from the NRF of Korea through the CRI (NRF-2012RIA3A2048842 to W.N.), GRL (NRF-2010-00353 to W.N.), and MSIP (NRF-2013RIA1A2062737 to K.-B.C.) and from JSPS KAKENHI (No. 16H02268 to S.F.).

■ REFERENCES

- (1) (a) Groves, J. T. *J. Inorg. Biochem.* **2006**, *100*, 434. (b) Nam, W. *Acc. Chem. Res.* **2007**, *40*, 522. (c) Hohenberger, J.; Ray, K.; Meyer, K. *Nat. Commun.* **2012**, *3*, 720. (d) Yin, G. *Acc. Chem. Res.* **2013**, *46*, 483. (e) Ray, K.; Pfaff, F. F.; Wang, B.; Nam, W. *J. Am. Chem. Soc.* **2014**, *136*, 13942. (f) Ray, K.; Heims, F.; Schwalbe, M.; Nam, W. *Curr. Opin. Chem. Biol.* **2015**, *25*, 159. (g) Chen, Z.; Yin, G. *Chem. Soc. Rev.* **2015**, *44*, 1083. (h) Nam, W. *Acc. Chem. Res.* **2015**, *48*, 2415. (i) Cook, S. A.; Hill, E. A.; Borovik, A. S. *Biochemistry* **2015**, *54*, 4167.
- (2) (a) Nam, W.; Lee, Y.-M.; Fukuzumi, S. *Acc. Chem. Res.* **2014**, *47*, 1146. (b) Cook, S. A.; Borovik, A. S. *Acc. Chem. Res.* **2015**, *48*, 2407. (c) Puri, M.; Que, L., Jr. *Acc. Chem. Res.* **2015**, *48*, 2443. (d) Neu, H. M.; Baglia, R. A.; Goldberg, D. P. *Acc. Chem. Res.* **2015**, *48*, 2754.
- (3) (a) Park, J.; Lee, Y.-M.; Nam, W.; Fukuzumi, S. *J. Am. Chem. Soc.* **2013**, *135*, 5052. (b) Park, J.; Morimoto, Y.; Lee, Y.-M.; Nam, W.; Fukuzumi, S. *Inorg. Chem.* **2014**, *53*, 3618. (c) Park, J.; Lee, Y.-M.; Ohkubo, K.; Nam, W.; Fukuzumi, S. *Inorg. Chem.* **2015**, *54*, 5806.
- (4) (a) Chen, J.; Lee, Y.-M.; Davis, K. M.; Wu, X.; Seo, M. S.; Cho, K.-B.; Yoon, H.; Park, Y. J.; Fukuzumi, S.; Pushkar, Y. N.; Nam, W. *J. Am. Chem. Soc.* **2013**, *135*, 6388. (b) Yoon, H.; Lee, Y.-M.; Wu, X.; Cho, K.-B.; Sarangi, R.; Nam, W.; Fukuzumi, S. *J. Am. Chem. Soc.* **2013**, *135*, 9186. (c) Chen, J.; Yoon, H.; Lee, Y.-M.; Seo, M. S.; Sarangi, R.; Fukuzumi, S.; Nam, W. *Chem. Sci.* **2015**, *6*, 3624. (d) Jung, J.; Kim, S.; Lee, Y.-M.; Nam, W.; Fukuzumi, S. *Angew. Chem., Int. Ed.* **2016**, *55*, 7450.
- (5) (a) Vaz, A. D. N.; McGinness, D. F.; Coon, M. J. *Proc. Natl. Acad. Sci. U. S. A.* **1998**, *95*, 3555. (b) Ruettinger, R. T.; Fulco, A. J. *J. Biol. Chem.* **1981**, *256*, 5728.
- (6) (a) Groves, J. T.; Subramanian, D. V. *J. Am. Chem. Soc.* **1984**, *106*, 2177. (b) Bartoli, J. F.; Brigaud, O.; Battioni, P.; Mansuy, D. *J. Chem. Soc., Chem. Commun.* **1991**, 440. (c) Suzuki, N.; Higuchi, T.; Urano, Y.; Kikuchi, K.; Uekusa, H.; Ohashi, Y.; Uchida, T.; Kitagawa, T.; Nagano, T. *J. Am. Chem. Soc.* **1999**, *121*, 11571.
- (7) (a) Song, W. J.; Ryu, Y. O.; Song, R.; Nam, W. *J. Biol. Inorg. Chem.* **2005**, *10*, 294. (b) Takahashi, A.; Kurahashi, T.; Fujii, H. *Inorg. Chem.* **2007**, *46*, 6227.
- (8) (a) De Visser, S. P.; Oglario, F.; Sharma, P. K.; Shaik, S. *J. Am. Chem. Soc.* **2002**, *124*, 11809. (b) De Visser, S. P.; Oglario, F.; Sharma, P. K.; Shaik, S. *Angew. Chem., Int. Ed.* **2002**, *41*, 1947. (c) Shaik, S.; De Visser, S. P.; Kumar, D. *J. Am. Chem. Soc.* **2004**, *126*, 11746.
- (9) Oloo, W. N.; Feng, Y.; Iyer, S.; Parmelee, S.; Xue, G.; Que, L., Jr. *New J. Chem.* **2013**, *37*, 3411.
- (10) (a) Kwon, Y. H.; Mai, B. K.; Lee, Y.-M.; Dhuri, S. N.; Mandal, D.; Cho, K.-B.; Kim, Y.; Shaik, S.; Nam, W. *J. Phys. Chem. Lett.* **2015**, *6*, 1472. (b) Dhuri, S. N.; Cho, K.-B.; Lee, Y.-M.; Shin, S. Y.; Kim, J. H.; Mandal, D.; Shaik, S.; Nam, W. *J. Am. Chem. Soc.* **2015**, *137*, 8623.
- (11) Mandal, D.; Ramanan, R.; Usharani, D.; Janardanan, D.; Wang, B.; Shaik, S. *J. Am. Chem. Soc.* **2015**, *137*, 722.
- (12) Wu, X.; Seo, M. S.; Davis, K. M.; Lee, Y.-M.; Chen, J.; Cho, K.-B.; Pushkar, Y. N.; Nam, W. *J. Am. Chem. Soc.* **2011**, *133*, 20088.
- (13) (a) Barman, P.; Vardhaman, A. K.; Martin, B.; Wörner, S. J.; Sastri, C. V.; Comba, P. *Angew. Chem., Int. Ed.* **2015**, *54*, 2095. (b) Leto, D. F.; Ingram, R.; Day, V. W.; Jackson, T. A. *Chem. Commun.* **2013**, *49*, 5378. (c) Wang, Y.; Shi, S.; Wang, H.; Zhu, D.; Yin, G. *Chem. Commun.* **2012**, *48*, 7832. (d) Shi, S.; Wang, Y.; Xu, A.; Wang,

H.; Zhu, D.; Roy, S. B.; Jackson, T. A.; Busch, D. H.; Yin, G. *Angew. Chem., Int. Ed.* **2011**, *50*, 7321. (e) Sawant, S. C.; Wu, X.; Cho, J.; Cho, K.-B.; Kim, S. H.; Seo, M. S.; Lee, Y.-M.; Kubo, M.; Ogura, T.; Shaik, S.; Nam, W. *Angew. Chem., Int. Ed.* **2010**, *49*, 8190. (f) Parsell, T. H.; Behan, R. K.; Green, M. T.; Hendrich, M. P.; Borovik, A. S. *J. Am. Chem. Soc.* **2006**, *128*, 8728. (g) Gupta, R.; Taguchi, T.; Lassalle-Kaiser, B.; Bominaar, E. L.; Yano, J.; Hendrich, M. P.; Borovik, A. S. *Proc. Natl. Acad. Sci. U. S. A.* **2015**, *112*, 5319.

(14) Ring-opened organic products as the major products, such as hexanedioic acid, were obtained, as reported previously: (a) Hirai, Y.; Kojima, T.; Mizutani, Y.; Shiota, Y.; Yoshizawa, K.; Fukuzumi, S. *Angew. Chem., Int. Ed.* **2008**, *47*, 5772. (b) Lee, Y.-M.; Dhuri, S. N.; Sawant, S. C.; Cho, J.; Kubo, M.; Ogura, T.; Fukuzumi, S.; Nam, W. *Angew. Chem., Int. Ed.* **2009**, *48*, 1803.

(15) The yield of the manganese(II) complex after the reaction of 1-(HOTf)₂ (1.0 mM) with cyclohexene (0.40 M) in CF₃CH₂OH/CH₃CN (*v/v* = 1:1) at 25 °C was determined to be 94(4)% by comparing the doubly integrated value with that of the authentic reference of [Mn^{II}(N4Py)]²⁺ (1.0 mM) in the presence of HOTf (50 mM).

(16) Luo, Y.-R. *Handbook of Bond Dissociation Energies in Organic Compounds*; CRC Press: New York, 2002.

(17) (a) Kadifachi, S. *Chem. Phys. Lett.* **1984**, *108*, 233. (b) von Bischof, P.; Heilbronner, E. *Helv. Chim. Acta* **1970**, *53*, 1677.

(18) The enhanced ET reactivity in olefin epoxidation reactions by HOTf-bound Mn^{IV}O species is under investigation in the laboratory and will be communicated shortly.

(19) (a) Cho, K.-B.; Shaik, S.; Nam, W. *J. Phys. Chem. Lett.* **2012**, *3*, 2851. (b) Chen, J.; Cho, K.-B.; Lee, Y.-M.; Kwon, Y. H.; Nam, W. *Chem. Commun.* **2015**, *51*, 13094. (c) Cho, K.-B.; Hirao, H.; Shaik, S.; Nam, W. *Chem. Soc. Rev.* **2016**, *45*, 1197.

(20) (a) Only two protons are equivalent with respect to the adiabatic C—H bond dissociation energy, which affects the transition state, albeit four are equivalent if relaxation energy is included. (b) Benson, S. W. *J. Am. Chem. Soc.* **1958**, *80*, 5151.

(21) The experiments and calculations hint that large tunneling may be involved (see SI, both experimental and DFT sections and Figure S16). However, due to the large error margins, further precise studies are required.

(22) Armarego, W. L. F.; Chai, C. L. L. *Purification of Laboratory Chemicals*, 6th ed; Pergamon Press: Oxford, U.K., 2009.

(23) Kaizer, J.; Klinker, E. J.; Oh, N. Y.; Rohde, J.-U.; Song, W. J.; Stubna, A.; Kim, J.; Münck, E.; Nam, W.; Que, L., Jr. *J. Am. Chem. Soc.* **2004**, *126*, 472.

(24) (a) Saltzman, H.; Sharefkin, J. G., Eds.; *Organic Syntheses*; Wiley: New York, 1973, Vol. V; p 658. (b) Dixon, N. E.; Lawrance, G. A.; Lay, P. A.; Sargeson, A. M.; Taube, H. *Inorg. Synth.* **1990**, *28*, 70.

(25) (a) Lubben, M.; Meetsma, A.; Wilkinson, E. C.; Feringa, B.; Que, L., Jr. *Angew. Chem., Int. Ed. Engl.* **1995**, *34*, 1512. (b) Duelund, L.; Hazell, R.; McKenzie, C. J.; Nielsen, L. P.; Toftlund, H. *J. Chem. Soc., Dalton Trans.* **2001**, 152. (c) Groni, S.; Dorlet, P.; Blain, G.; Bourcier, S.; Guillot, R.; Anxolabéhère-Mallart, E. *Inorg. Chem.* **2008**, *47*, 3166.

(26) Yoon, H.; Morimoto, Y.; Lee, Y.-M.; Nam, W.; Fukuzumi, S. *Chem. Commun.* **2012**, *48*, 11187.

(27) Kohn, W.; Sham, L. J. *Phys. Rev.* **1965**, *140*, A1133.

(28) (a) Becke, A. D. *Phys. Rev. A: At., Mol., Opt. Phys.* **1988**, *38*, 3098. (b) Becke, A. D. *J. Chem. Phys.* **1993**, *98*, 1372. (c) Becke, A. D. *J. Chem. Phys.* **1993**, *98*, 5648. (d) Lee, C.; Yang, W.; Parr, R. G. *Phys. Rev. B: Condens. Matter Mater. Phys.* **1988**, *37*, 785.

(29) Frisch, M. J.; Trucks, G. W.; Schlegel, H. B.; Scuseria, G. E.; Robb, M. A.; Cheeseman, J. R.; Scalmani, G.; Barone, V.; Mennucci, B.; Petersson, G. A.; Nakatsuji, H.; Caricato, M.; Li, X.; Hratchian, H. P.; Izmaylov, A. F.; Bloino, J.; Zheng, G.; Sonnenberg, J. L.; Hada, M.; Ehara, M.; Toyota, K.; Fukuda, R.; Hasegawa, J.; Ishida, M.; Nakajima, T.; Honda, Y.; Kitao, O.; Nakai, H.; Vreven, T.; Montgomery, J. A.; Peralta, J. E., Jr.; Ogliaro, F.; Bearpark, M.; Heyd, J. J.; Brothers, E.; Kudin, K. N.; Staroverov, V. N.; Keith, T.; Kobayashi, R.; Normand, J.; Raghavachari, K.; Rendell, A.; Burant, J. C.; Iyengar, S. S.; Tomasi, J.;

Cossi, M.; Rega, N.; Millam, J. M.; Klene, M.; Knox, J. E.; Cross, J. B.; Bakken, V.; Adamo, C.; Jaramillo, J.; Gomperts, R.; Stratmann, R. E.; Yazyev, O.; Austin, A. J.; Cammi, R.; Pomelli, C.; Ochterski, J. W.; Martin, R. L.; Morokuma, K.; Zakrzewski, V. G.; Voth, G. A.; Salvador, P.; Dannenberg, J. J.; Dapprich, S.; Daniels, A. D.; Farkas, O.; Foresman, J. B.; Ortiz, J. V.; Cioslowski, J.; Fox, D. J. *Gaussian 09, Revisions B.01 and D.01*; Gaussian, Inc.: Wallingford CT, 2010.

(30) (a) Hay, P. J.; Wadt, W. R. *J. Chem. Phys.* **1985**, *82*, 270. (b) Hay, P. J.; Wadt, W. R. *J. Chem. Phys.* **1985**, *82*, 299.

(31) *Jaguar, version 7.7*, Schrödinger, L. L. C., New York, NY, 2010.

(32) (a) Hehre, W. J.; Ditchfield, R.; Pople, J. A. *J. Chem. Phys.* **1972**, *56*, 2257. (b) Francl, M. M.; Pietro, W. J.; Hehre, W. J.; Binkley, J. S.; Gordon, M. S.; DeFrees, D. J.; Pople, J. A. *J. Chem. Phys.* **1982**, *77*, 3654.

(33) (a) Johansson, A. J.; Blomberg, M. R. A.; Siegbahn, P. E. M. *J. Chem. Phys.* **2008**, *129*, 154301. (b) Johansson, A. J.; Blomberg, M. R. A.; Siegbahn, P. E. M. *J. Phys. Chem. C* **2007**, *111*, 12397.

(34) Cossi, M.; Rega, N.; Scalmani, G.; Barone, V. *J. Comput. Chem.* **2003**, *24*, 669.

(35) Weigend, F.; Ahlrichs, R. *Phys. Chem. Chem. Phys.* **2005**, *7*, 3297.

(36) Harvey, J. N.; Aschi, M.; Schwarz, H.; Koch, W. *Theor. Chem. Acc.* **1998**, *99*, 95.